

Pinpointing Delay and Forwarding Anomalies Using Large-Scale Traceroute Measurements

Romain Fontugne
IIJ Research Lab

Emile Aben
RIPE NCC

Cristel Pelsser
University of Strasbourg / CNRS

Randy Bush
IIJ Research Lab

ABSTRACT

Understanding network health is essential to improve Internet reliability. For instance, detecting disruptions in peer and provider networks facilitates the identification of connectivity problems. Currently this task is time consuming for network operators. It involves a fair amount of manual observation because operators have little visibility into other networks. In this paper we leverage the RIPE Atlas measurement platform to monitor and analyze network conditions. We propose a set of complementary methods to detect network disruptions from traceroute measurements. A novel method of detecting changes in delays is used to identify congested links, and a packet forwarding model is employed to predict traffic paths and to identify faulty routers in case of packet loss. In addition, aggregating results from each method allows us to easily monitor a network and identify coordinated reports manifesting significant network disruptions, reducing uninteresting alarms. Our contributions consist of a statistical approach providing robust estimation for Internet delays and the study of hundreds of thousands link delays. We present three cases demonstrating that the proposed methods detect real disruptions and provide valuable insights, as well as surprising findings, on the location and impact of identified events.

1. INTRODUCTION

The Internet’s decentralized design allows many disparate networks to cooperate and provides resilience to failure. However, significant network disruptions inevitably degrade users’ connectivity. The first step to improve reliability is to understand the health of the current Internet. While network operators may have an understanding of their own network’s condition, understanding conditions in the global multi-provider Internet remains a crucial task. Monitoring multiple networks’ health is difficult, and far too often requires many manual observations. For example, network operators’ group mailing lists are a common way to signal and share knowledge about network disruptions [9]. Manual network measurements, such as ping and traceroute assist in diagnosing connectivity issues from a few vantage points but they suffer from poor visibility.

We investigate the potential of a large-scale measurement platform, RIPE Atlas [1], to systematically detect and locate network disruptions. The widespread deployment of Atlas probes provides an extensive view of the Internet that has proved beneficial for postmortem reports [4, 5, 26]. Designing automated detection tools for such large-scale platforms is challenging. The high variability of network performance metrics, such as round trip time (RTT), is a key obstacle for reliable event detection [31]. Beyond detecting network disruptions, pinpointing their location is often challenging due to traffic asymmetry and packet loss.

We examine these challenges (Section 3) and propose methods to monitor the health of the vast number of networks probed by Atlas traceroutes. First, we devise a method to monitor RTT from traceroute results and report links with unusual delays (Section 4). This method takes advantage of the wide deployment of Atlas by monitoring links from numerous vantage points, accurately measuring delay changes. Second, we explore a packet forwarding model to learn and predict forwarding behavior and pinpoint faulty routers experiencing sudden packet loss (Section 5). Finally, we present a technique to aggregate these signals per network and detect inter-related events (Section 6). These methods are all based on robust statistics which cope with outliers commonly found in traceroute measurements.

The contributions of this work reside in the statistical approach to monitor Internet delays. Despite noisy RTT measurements, the introduced delay estimator infers very stable link delays and permits accurate predictions for anomaly detection. It also enables the monitoring of delays and forwarding patterns for hundreds of thousands links.

To validate the proposed methods we analyze three significant network disruptions detected in 2015 (Section 7), each demonstrating key benefits of our techniques. The first exhibits the impact of a DDoS infrastructure attack. The second shows congestion in a tier-1 ISP caused by inadvertent rerouting of significant traffic. And the last presents connectivity issues at an

Internet Exchange due to a technical fault.

2. DATASET

To monitor a vast number of networks our study requires a vast number of vantage points collecting network performance data. With its impressive spread across the globe and almost 10,000 probes constantly connected, RIPE Atlas is the best candidate. Atlas performs, among others, two classes of repetitive measurements providing an extensive collection of traceroute data. The first type is called *builtin* measurements and consists of traceroutes from all Atlas probes to instances of the 13 DNS root servers every 30 minutes. Due to the wide distribution of probes and the anycast DNS root server deployment, this is actually to over 500 root server instances. The second type, the *anchoring* measurements, are traceroutes to 189 collaborative servers (super probes) from about 400 probes every 15 minutes. All measurements employ Paris traceroute [8] to mitigate issues raised by load balancers and link aggregation.

We have analyzed the builtin and anchoring measurements results from May 1st to December 31st 2015. This corresponds to a total of 2.8 billion IPv4 traceroutes (1.2 billion IPv6 traceroutes) from a total of 11,538 IPv4 probes (4,307 IPv6 probes) connected within the eight studied months.

As our study relies solely on traceroute results the scope and terminology of this paper are constrained to the IP layer. That is, a link refers to a pair of IP addresses rather than a physical cable.

3. CHALLENGES AND RELATED WORK

Monitoring network performance with traceroute raises three key challenges. In this section, we present these challenges, discuss how they were tackled in previous work, and give hints of our approach.

3.1 Traffic asymmetry

Traceroute measurements are a rich source of information to monitor Internet delays. They reveal the path to a destination and provide RTT values for every router on this path. Each RTT value is the sum of the time spent to reach a certain IP address and the travel time for the corresponding reply. Due to the asymmetry and diversity of Internet routes [40, 48] the paths taken by the forwarding and returning packets might be different, and traceroute is unable to reveal IP addresses on the return path. Furthermore, path asymmetry is very common in the Internet; past studies report about 90% of AS-level routes as asymmetric [37, 12]. For these reasons one should take particular care when comparing RTT values for different hops.

For instance, quantifying the delay between two adjacent hops can be a baffling problem. Figure 1 illus-

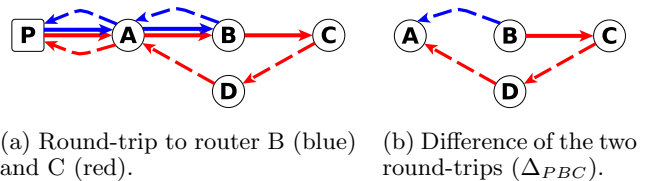


Figure 1: Example of traceroute results with different return paths. P is the probe initiating the traceroute. A , B , and C are routers reported by traceroute. D is a router on the return path, unseen in the traceroute. Solid lines represent the forward paths, dashed the return paths.

trates this by breaking down the RTT from the probe P to router B (blue in Figure 1a) and the one to the following hop, router C (red in Figure 1a). The solid lines represent the forward path exposed by traceroute, and the dotted the unrevealed return path. If we want to measure the delay between routers B and C using only the information provided by traceroute (i.e. solid lines in Figure 1), one is tempted to compute the delay between B and C as the difference between the RTT to B the one to C . But the resulting value is ambiguous when forward and return paths are asymmetric. Packets returning from C are not going through B but D , a router not seen on the forward path. If one is monitoring the difference between the two RTTs over time and identifying an abnormal increase, then it is unclear if this increase is due to abnormal delay on link BC , CD , DA , or BA (Figure 1b).

Previous studies approach this problem with reverse traceroute techniques that take advantage of IP options to track the return path [19, 27]. Using these techniques Luckie et al. [23] filter out routers with different forward and return paths and characterize congestion for the remaining routers. Due to the limitations of these reverse traceroute techniques [11] and the strong asymmetry of Internet traffic [12], they could study only 29.9% of the routers observed in their experiments.

Coordinated probing from both ends of the path is another way to reveal asymmetric paths and corresponding delays [13, 10]. However, coordinated probing requires synchronized control on hosts located at both ends of the path, which is difficult in practice and limits the probing surface.

Tulip [25] and cing [7] bypass the traffic asymmetry problem by measuring delays with ICMP options but require routers to implement these options.

In Section 4.1 we review the asymmetric paths problem and propose a new approach that takes advantage of multiple probes and path diversity to accurately monitor delay fluctuations for links visited from different vantage points.

3.2 RTT variability

As packets travel along multiple links, routers, queues, and middleboxes, they are exposed to multiple sources of delay that result in complex RTT dynamics. This phenomenon has been studied since the early years of the Internet and is still of interest as comprehensive understanding of Internet delays is a key step to understand network conditions [33, 15, 38, 30]. Simply stated, monitoring Internet delays is a delicate task because RTT samples are contaminated by various noise sources. In the literature, RTTs are monitored differently depending on study concerns. Minimum RTT values reveal propagation and transmission delays but filter out delays from transient congestion, so are commonly used to compute geographic distance in IP geolocation systems [18, 46]. Studies focusing on queuing delays usually rely on RTT percentiles [6, 28], there is however no convention to choose specific quantiles. For instance, Chandrasekaran et al. [10] define the 10th percentile as the *baseline* RTT and the 90th percentile as *spikes* (i.e. sudden RTT increases), in the same study they also report results for the 5th and 95th percentile.

In this paper, we monitor the median RTT (i.e. 50th percentile) which accounts for high delays only if they represent the majority of the RTT samples. Section 4.2 presents the other robust statistics we employ to analyze RTT measurements.

3.3 Packet loss

Delay is an important but insufficient indicator to identify connectivity issues. In worst-case scenarios networks fail to transmit packets and the lack of samples clouds delay measurements. Increases in delay and packet loss are not necessarily correlated [28]. Congestion provides typical examples where both metrics are affected [39], but routers implementing active queue management (e.g. Random Early Detection [14]) can mitigate this [23] as the routers drop packets to avoid significant delay increase. Other examples include bursts of lost packets on routing failure [42]. In this paper, we stress that a comprehensive analysis of network conditions must track both network delay and packet loss.

Packet loss is sometimes overlooked by congestion detection systems. For instance, Pong [13] and TSLP [23] probe routers to monitor queueing delays but users are left with no guidance in the case of lost probes. Consequently, studies using these techniques tend to ignore incomplete experiments caused by lost packets (e.g. 25% of the dataset is disregarded in ref. [10]), and potentially misses major events.

Detecting packet loss is of course an easy task; the key difficulty is to locate where the packets are dropped. Several approaches have been previously proposed to address this. The obvious technique is to continuously probe routers, or networks, and report packet loss or

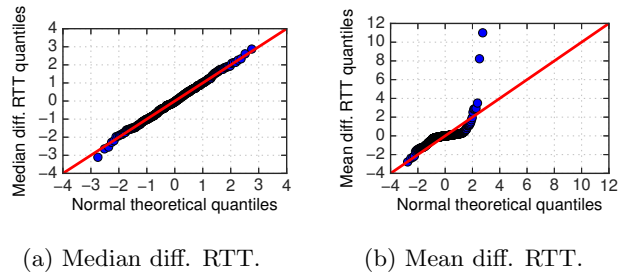


Figure 3: Normality tests for the same data as Figure 2. Q-Q plots of the median and mean differential RTT versus a normal distribution.

disconnections [25, 32]. This is, however, particularly greedy in terms of network resources, hence, difficult to deploy for long-term measurements. Another approach employs both passive and active monitoring techniques to build end-to-end reference paths, passively detect packet loss, and actively locate path changes [47]. Approaches using only passive measurements are also possible; although wide coverage requires collection of flow statistics from many routers [17].

In Section 5 we introduce a forwarding anomaly detection method that complements the proposed RTT analysis method (Section 4). It analyzes traceroute data and creates reference forwarding patterns for each router. These patterns are used to locate routers that drop packets in abnormal situations.

4. IN-NETWORK DELAYS

This section describes our approach to detecting abnormal delay changes in wide-area traceroute measurements. To address the traffic asymmetry challenge we propose monitoring a link’s delay using Atlas probes from different ASs (Section 4.1). Then, we use a robust detector to identify abnormal delay changes (Section 4.2).

4.1 Differential RTT

As stated in Section 3.1, locating delay changes from traceroute data is challenging because of traffic asymmetry. We address this challenge by taking advantage of the topographically-wide deployment of Atlas probes.

Let’s revisit the example of Figure 1 and introduce our notation. RTT_{PB} stands for the round-trip-time from the probe P to the router B . The difference between the RTT from P to the two adjacent routers, B and C , is called differential RTT and noted Δ_{PBC} . The differential RTT of Figure 1b is decomposed as follows:

$$\Delta_{PBC} = RTT_{PC} - RTT_{PB} \quad (1)$$

$$= \delta_{BC} + \delta_{CD} + \delta_{DA} - \delta_{BA} \quad (2)$$

$$= \delta_{BC} + \varepsilon_{PBC} \quad (3)$$

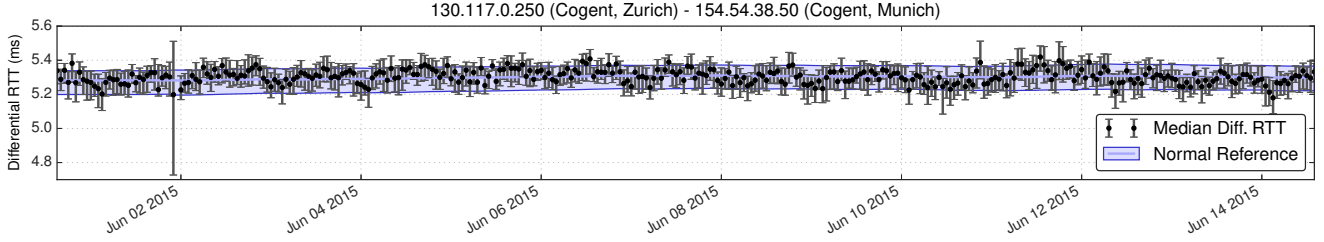


Figure 2: Example of median differential RTTs for a pair of IP addresses from Cogent Communications (AS174). Every median differential RTT is computed from a 1-hour time window, the error bars are the 95% confidence intervals obtained by the Wilson Score and the normal reference is derived from these intervals.

where δ_{XY} is the delay for the link XY and ε_{PBC} is the time difference between the two return paths.

Δ_{PBC} alone gives a poor indication of the delay of link BC because the two components, δ_{BC} and ε_{PBC} , are not dissociable. Nonetheless, these two variables are independent and controlled by different factors. The value of δ_{BC} depends only on the states of routers B and C , and is unrelated to the monitoring probe P . In contrast, ε_{PBC} is intimately tied to P , the destination for the two return paths.

Assuming that we have a pool of n probes $P_i, i \in [1, n]$, all with different return paths from B and C ; then, the differential RTTs for all probes, Δ_{P_iBC} , share the same δ_{BC} but have independent ε_{P_iBC} values. The independence of ε_{P_iBC} also means that the distribution of Δ_{P_iBC} is expected to be stable over time if δ_{BC} is constant. In contrast, significant changes in δ_{BC} influence all differential RTT values and the distribution of Δ_{P_iBC} shifts along with the δ_{BC} changes. Monitoring these shifts allows us to discard uncertainty from return paths (ε_{P_iBC}) and focus only on delay changes for the observed link (δ_{BC}).

Now let's assume the opposite scenario where B always pushes returning packets to A , the previous router on the forwarding path (see Figure 1). In this case ε_P represents the delay between B and A ; hence, Equation 3 simplifies as:

$$\Delta_{PAB} = \delta_{AB} + \delta_{BA}. \quad (4)$$

Meaning the differential RTT Δ_{PAB} stands for the delays between router A and B in both directions. This scenario is similar to the one handled by TSLP [23], and in the case of delay changes, determining which one of the two directions is affected requires extra measurements (see [23] Section 3.4).

In both scenarios, monitoring the distribution of differential RTTs permits detection of delay changes between adjacent routers. Notice that we are exclusively looking at differential RTT fluctuations rather than their absolute values. The absolute values of differential RTTs

can be misleading; as they include error from return paths, they cannot account for the actual link delay. In our experiments we observe negative differential RTTs, $\Delta_{PXY} < 0$, meaning that Y has a lower RTT than X due to traffic asymmetry (see Figure 6c and 6d).

4.2 Delay change detection

The theoretical observations of the previous section are the fundamental mechanisms of our delay change detection system. Namely, the system collects all traceroutes initiated from a 1-hour time bin and performs the five following steps: (1) Compute the differential RTTs for each link (i.e. pair of adjacent IP addresses observed in traceroutes). (2) Links that are observed from only a few ASs are discarded. (3) The differential RTT distributions of remaining links are characterized with nonparametric statistics, (4) and compared to computed references in order to identify abnormal delay changes. (5) The references are updated with the latest differential RTT values. The same steps are repeated to analyze the subsequent time bins. The remainder of this section details steps for handling differential RTTs (i.e. steps 1, 3, 4, and 5). Step 2 is a filtering process to discard links with ambiguous differential RTTs and is discussed later in Section 4.3.

4.2.1 Differential RTTs computation

The first step is calculating the difference between RTT values measured for adjacent routers. Let X and Y be two adjacent routers observed in a traceroute initiated by the probe P . The traceroute yields from one to three values for RTT_{PX} and RTT_{PY} . The differential RTT samples, Δ_{PXY} are computed for all possible combinations $RTT_{PY} - RTT_{PX}$; hence, we have from one to nine differential RTT samples per probe. In the following, all differential RTTs obtained with every probe are denoted Δ_{XY} , or simply Δ when confusion is not likely.

4.2.2 Differential RTTs characterization

This step characterizes the differential RTTs Δ_{XY} obtained in the previous step. Significant deviation of Δ_{XY} from the reference implies abnormal delays for link XY . In practice, these anomalies are detected using a variant of the Central Limit Theorem (CLT). The original CLT states that, regardless the distribution of Δ_{XY} , its arithmetic mean is normally distributed if the number of samples is relatively large. If the underlying process changes, namely the delays for X and Y in our case, then the resulting mean values deviate from the normal distribution and are detected as anomalous.

Our preliminary experiments suggest that the frequent outlying values found in RTT measurements greatly affect the computed mean values; thus an impractical number of samples is required for the CLT to hold. To address this we replace the arithmetic mean by the median. This is much more robust to outlying values. This variant of the CLT also requires less samples to converge to the normal distribution [44].

Figure 2 depicts the hourly median differential RTTs (black dots) obtained for a pair of IP addresses from Cogent networks (AS174) during two weeks in June 2015. This link is observed by 95 different probes between June 1st and June 15th. The raw differential RTT values exhibit large fluctuations; the standard deviation ($\sigma = 12.2$) is almost three times larger than the average value ($\mu = 4.8$). Despite this variability, the median differential RTT is remarkably steady, all values lie between 5.2 and 5.4 milliseconds (Figure 2). Therefore, using the median allows us to accurately monitor delays and detect small changes on the order of a millisecond.

We confirm that the employed CLT variant holds very well in this experiment. Figure 3a compares the quantiles of the computed medians to those of a normal distribution. As all points are in line with the $x = y$ diagonal, the computed median differential RTTs fit a normal distribution quite well. In contrast, the mean differential RTT is not normally distributed (Figure 3b). By manually inspecting the raw RTT values, we found 125 outlying values (i.e. greater than $\mu + 3\sigma$) that greatly alter the mean. These outliers are isolated events spread throughout the two weeks, and are attributed to measurement errors. Despite the large number of probing packets going through this link, the mean differential RTTs are greatly altered by these few outliers. These observations support our choice for the CLT variant against the original CLT.

To account for uncertainty in the computed medians, we also calculate confidence intervals. In the case of the median, confidence intervals are usually formulated as a binomial calculation and are distribution free [16]. In this work we approximate this calculation with the Wilson score [45] since it has been reported to perform well even with a small number of samples [29]. The

Wilson score is defined as follows:

$$w = \frac{1}{1 + \frac{1}{n}z^2} \left(p + \frac{1}{2n}z^2 \pm z\sqrt{\frac{1}{n}p(1-p) + \frac{1}{4n^2}z^2} \right) \quad (5)$$

where n is the number of samples, the probability of success p is set to 0.5 in the case of the median, and z is set to 1.96 for a 95% confidence level. The Wilson score provides two values, hereafter called w_l and w_u , ranging in $[0, 1]$. Multiplying w_l and w_u by the number of samples gives the rank of the lower and upper bound of the confidence interval, namely $l = nw_l$ and $u = nw_u$.

For example, let $\Delta^{(1)}, \dots, \Delta^{(n)}$ be the n differential RTT values obtained for a single link, and assume these values are ordered, i.e. $\Delta^{(1)} \leq \Delta^{(2)} \leq \dots \leq \Delta^{(n)}$. Then, for these measures the lower and upper bound of the confidence interval are given respectively by $\Delta^{(l)}$ and $\Delta^{(u)}$.

Based solely on order statistics, the Wilson score produces asymmetric confidence intervals in the case of skewed distributions, which is common for RTT distributions [15]. Further, unlike a simple confidence interval based on the standard deviation, this non-parametric technique takes advantage of order statistics to discard undesirable outliers.

The whiskers in Figure 2 depict the confidence intervals obtained for the Cogent link discussed above. These intervals are consistent over time and show that the median differential RTT for this link reliably falls between 5.1 and 5.5 milliseconds. The large confidence interval reported on June 1st illustrates an example where RTT measures are noisier than other days; yet we stress that the median value and confidence interval are compatible with those obtained by other time bins. The following section describes how we identify statistically deviating differential RTTs.

4.2.3 Anomalous delays detection

A delay change results in a differential RTT distribution shift, thus a significant change in the corresponding median differential RTT value. Assume we have a reference median and its corresponding 95% confidence interval that represents the usual delay measured for a certain link (the calculation of such reference is addressed in Section 4.2.4). To measure if the difference between an observed median and the reference is statistically significant we examine the overlap between their confidence intervals. If the two confidence intervals are not overlapping, we conclude that there is a statistically significant difference between the two medians [36] so we report the observed median as anomalous. As a rule of thumb we discard anomalies where the difference between the two medians is lower than 1ms (in our experiments these account for 3% of the reported links). Although statistically meaningful, these small anomalies are less relevant for the study of network disruption.

The deviation from the normal reference is given by the gap between the two confidence intervals. Let $\bar{\Delta}^{(l)}$ and $\bar{\Delta}^{(u)}$ be, respectively, the lower and upper bound of the reference confidence interval and $\bar{\Delta}^{(m)}$ the reference median. Then, the deviation from the normal reference of the observed differential RTTs, Δ , is defined as:

$$d(\Delta) = \begin{cases} \frac{\Delta^{(l)} - \bar{\Delta}^{(u)}}{\bar{\Delta}^{(u)} - \bar{\Delta}^{(m)}}, & \text{if } \bar{\Delta}^{(u)} < \Delta^{(l)} \\ \frac{\bar{\Delta}^{(l)} - \Delta^{(u)}}{\bar{\Delta}^{(m)} - \bar{\Delta}^{(l)}}, & \text{if } \bar{\Delta}^{(l)} > \Delta^{(u)} \\ 0, & \text{otherwise.} \end{cases} \quad (6)$$

This deviation represents the gap separating the two confidence intervals and is relative to the usual uncertainty measured by the reference confidence interval. Values close to zero represent small delay changes while large values represent important changes.

Figure 2 exhibits confidence intervals along with the corresponding normal reference. As the reference intersects with all confidence intervals, no anomaly is reported for this link. The evaluation section presents several examples of anomalies. For example, Figure 6c depicts two confidence intervals deviating from the normal reference on November 30th.

4.2.4 Normal reference computation

In the previous section we assumed having a reference differential RTT distribution for each link. We will now see how to compute them. The goal of the references is to characterize the usual delays of observed links. As median differential RTT values are normally distributed (Section 4.2.2), the expected median value for a link is simply obtained as the arithmetic mean of previously observed medians for that link. Because anomalies might impair mean values and make them irrelevant as references, we employ exponential smoothing to estimate the medians' mean value to reduce the impact of anomalies. Let $m_t = \Delta^{(m)}$ be the median differential RTT observed for a certain link in time bin t , and, $\bar{m}_{t-1} = \bar{\Delta}^{(m)}$ be the reference median computed with median differential RTTs observed in the previous time bin, $t - 1$. Then the next reference median, \bar{m}_t is defined as:

$$\bar{m}_t = \alpha m_t + (1 - \alpha) \bar{m}_{t-1} \quad (7)$$

The only parameter for the exponential smoothing, $\alpha \in (0, 1)$, controls the importance of new measures as opposed to the previously observed ones. In our case a small α value is preferable as it allows us to mitigate the impact of anomalous values. The initial value of the reference, \bar{m}_0 , is quite important when α is small. We arbitrarily set this value using the first three time bins, namely, $\bar{m}_0 = \text{median}(m_1, m_2, m_3)$.

For the reference confidence interval, the lower and upper bounds (resp. $\bar{\Delta}^{(l)}$ and $\bar{\Delta}^{(u)}$) are computed in

the same way as the reference median ($\bar{\Delta}^{(m)}$) but using the boundary values given by the Wilson score (i.e. $\Delta^{(l)}$ and $\Delta^{(u)}$).

4.3 Probe diversity

The above differential RTT analysis applies only under certain conditions. Section 4.1 shows that monitoring Δ_{XY} reveals delay changes between router X and Y only if the following hold true. (1) The link is monitored by several probes and the return paths to these probes are disparate. (2) All returning packets are also going through the link XY but in the opposite direction. Therefore, if we have differential RTT values Δ_{XY} from ten probes which share the same asymmetric return path, we cannot distinguish delay changes on XY from delay changes in the return path, so these differential RTT values cannot be used.

We propose a technique to filter out ambiguous differential RTTs. We avoid links monitored only by probes from the same AS (thus more likely to share the same return path due to common inter-domain routing policies), but instead, take advantage of the world-wide deployment of Atlas probes and focus on links monitored from a variety of ASs. We devise two criteria to control the diversity of probes monitoring a link.

The first criterion filters out links that are monitored by probes from less than 3 different ASs. The value 3 is empirically found and could be increased for more conservative studies. This simple criterion allows us to avoid ambiguous results when links are monitored from only a few ASs, but is insufficient to control probe diversity. For instance, a link XY is monitored by 100 probes located in 5 different ASs but 90 of these probes are in the same AS. Then, the corresponding differential RTT distribution is governed by the return path shared by these 90 probes, meaning that delay changes on this return path are indistinguishable from delay changes on XY .

The second criterion finds links with an unbalanced number of probes per AS. Measuring such information dispersion is commonly addressed using normalized entropy. Let $A = \{a_i | i \in [1, n]\}$ be the number of probes for each of the n ASs monitoring a certain link, then the entropy $H(A)$ is defined as:

$$H(A) = -\frac{1}{\ln n} \sum_{i=1}^n P(a_i) \ln P(a_i). \quad (8)$$

Low entropy values, $H(A) \simeq 0$, mean that most of the probes are concentrated in one AS, and, high entropy values, $H(A) \simeq 1$, indicate that probes are evenly dispersed among ASs. This second criterion ensures that analyzed links feature an entropy $H(A) > 0.5$.

If the second criterion is not met (i.e. $H(A) \leq 0.5$) the link is not discarded. Instead, a probe from the most represented AS (namely AS i such as $a_i = \max(A)$) is

randomly selected and discarded, thus increasing the value of $H(A)$. This process is repeated until $H(A) > 0.5$, hence the corresponding differential RTTs are relevant for our analysis.

5. FORWARDING ANOMALIES

Latency is a good indicator of network health, but deficient in certain cases. For example, if traffic is rerouted or probing packets are lost then the lack of RTT samples impede delay analysis. We refer to these cases as forwarding anomalies. In this section we introduce a method to detect forwarding anomalies, complementing the delay analysis method presented in Section 4.

A forwarding anomaly can be legitimate, for example rerouted traffic, but it can also highlight compelling events such as link failures or routers dropping packets. Using traceroute data such events appear as routers vanishing from our dataset. So our approach monitors where packets are forwarded and constructs a simple packet forwarding model (Section 5.1). This model allows us to predict next hop IP addresses in traceroutes, thus detecting and identifying disappearing routers (Section 5.2).

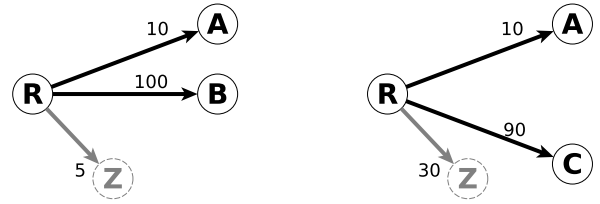
5.1 Packet forwarding model

The proposed packet forwarding model learns from past traceroute data the next hops usually observed after each router. Because routers determine next hops based on the packet destination IP address, we compute a different model for each traceroute target.

Let us consider traceroutes from all probes to a single destination in the same time bin. For each router in these traceroutes we record the adjacent nodes to which packets have been forwarded. We distinguish two types of next hop, responsive and unresponsive ones. The responsive next hops are visible in traceroutes as they send back ICMP messages when a packet TTL expires. Next hops that do not send back ICMP packets to the probes or drop packets are said to be unresponsive and are indissociable in traceroutes.

Figure 4a illustrates the example of a router R with two responsive hops, A and B , and unresponsive hops, Z . The packet forwarding pattern of this router is formally defined as a vector where each element represents a next hop and the value of the element is the number of packets transmitted to that hop. For Figure 4a the forwarding pattern of R is $F^R = [10, 100, 5]$.

To summarize router R 's usual patterns and to update this reference with new patterns, we again employ exponential smoothing (see Equation 9). Let $F_t^R = \{p_i | i \in [1, n]\}$ be the forwarding pattern for router R at time t and $\bar{F}_{t-1}^R = \{\bar{p}_i | i \in [1, n]\}$ be the reference computed at time $t-1$. These two vectors are sorted such as p_i and \bar{p}_i correspond to the same next hop i . If the hop i is unseen at time t then $p_i = 0$, similarly, if



(a) Usual forwarding pattern. (b) Anomalous pattern.

Figure 4: Two forwarding patterns for router R . A, B , and C are next hops identified in traceroutes. Z shows packet loss and next hops that are unresponsive to traceroute.

the hop i is observed for the first time at time t then $\bar{p}_i = 0$. The reference \bar{F}_{t-1}^R is updated with the new pattern F_t^R as follows:

$$\bar{F}_t^R = \alpha F_t^R + (1 - \alpha) \bar{F}_{t-1}^R. \quad (9)$$

As in Section 4.2.4, a small α value allows us to mitigate the impact of anomalous values. The reference \bar{F}_t^R represents the usual forwarding pattern for router R and is the normal reference used for the anomaly detection method discussed in the next section. A reference \bar{F}_t^R is valid only for a certain destination IP address. In practice we compute a different reference for each traceroute target; thus, several references are maintained for a single router.

5.2 Forwarding anomaly detection

5.2.1 Correlation analysis

Detecting anomalous forwarding patterns consists of identifying patterns F that deviate from the computed normal reference \bar{F} . In normal conditions we expect a router to forward packets as they did in past observations. In other words, we expect F and \bar{F} to be linearly correlated. This linear dependence is easily measurable as the Pearson product-moment correlation coefficient of F and \bar{F} , hereafter denoted as $\rho_{F, \bar{F}}$. The values of $\rho_{F, \bar{F}}$ range in $[-1, 1]$. Positive values mean that the forwarding patterns expressed by F and \bar{F} are compatible, whereas, negative values indicate opposite patterns hence forwarding anomalies. Therefore, all patterns F with a correlation coefficient $\rho_{F, \bar{F}} < \tau$ are reported as anomalous. In our experiments we empirically set $\tau = -0.2$. Conservative results can be obtained with lower τ values, but higher values are best avoided as $\rho > -0.2$ represents very weak anti-correlation.

5.2.2 Anomalous next hop identification

When a forwarding pattern F is reported as anomalous, it means that the proportions of packets sent to

next hops are different from those observed in past data. Furthermore, an anomalous pattern can be caused by just a few aberrant next hops. We devise a metric to identify hops that are responsible for forwarding pattern changes. Let $F = \{p_i | i \in [1, n]\}$ be an anomalous pattern and $\bar{F} = \{\bar{p}_i | i \in [1, n]\}$ the computed normal reference. Then we quantify the responsibility of the next hop i to the pattern change as:

$$r_i = -\rho_{F, \bar{F}} \frac{p_i - \bar{p}_i}{\sum_{j=1}^n |p_j - \bar{p}_j|}. \quad (10)$$

The responsibility metric r_i ranges in $[-1, 1]$. Values close to zero means that the next hop i receives an usual number of packets thus it is likely not responsible for the pattern change. On the other hand, values deviating from 0 indicate anomalous next hops. Positive values stand for hops that are newly observed, while negative values represent hops with an unusually low number of packets.

For example, assume Figure 4a depicts \bar{F}^R , the computed normal reference for router R , and Figure 4b illustrates F^R , the latest forwarding pattern observed. The correlation coefficient for these patterns, $\rho_{F^R, \bar{F}^R} = -0.6$, is lower than the threshold τ thus F^R is reported as anomalous. The responsibility scores for A, B, C and Z are, respectively, 0, -0.28 , 0.25 , and 0.07 . Suggesting that packets are ordinarily transmitted to A and Z , but, the number of packets to B is abnormally low while the count to C is exceptionally high. In other words traffic usually forwarded to B is now going through C . In the case of a next hop dropping a significant number of packets, the responsibility score of this hop will be negative while the score of Z will be large.

6. DETECTION OF MAJOR NETWORK DISRUPTIONS

The proposed delay analysis method (Section 4) and packet forwarding model (Section 5) are both designed to report anomalies found in large-scale traceroute measurements. With RIPE Atlas these methods allow us to monitor hundreds of thousands links and potentially obtain a large number of alarms (i.e. either delay changes or forwarding anomalies). Investigating each alarm can be very tedious and time consuming. In this section we introduce a simple technique to aggregate alarms and report only outstanding network disruptions.

6.1 Alarm aggregation

Major network disruptions are characterized by either a large-scale alteration of numerous links or exceptional connectivity issues at a single location. We wish to emphasize both by aggregating alarms based on their temporal and spatial characteristics. The temporal grouping of alarms allows us to highlight large-scale events impacting many routers at the same time. Similarly,

collecting alarms that are topologically close allows us to emphasize network disruptions bound to a particular entity. In early experiments we have tried several spatial aggregations, including geographical ones, and found that grouping alarms per AS is relevant because most significant events are contained within one or a few ASs.

Consequently, we group delay change alarms by the reported IP pair and forwarding anomalies by the next hops IP addresses. The IP to AS mapping is done using longest prefix match, and alarms with IP addresses from different ASs are assigned to multiple groups.

Alarms from each AS are then processed to compute two time series representing the severity of reported anomalies thus the AS conditions. The severity of anomalies is measured differently for delay change and packet forwarding alarms. For delay changes the severity is measured by the deviation from the normal reference, $d(\Delta)$ (Equation 6). Severity of forwarding anomalies is given by r_i , the responsibility score of the reported next hop i (Equation 10). Thereby, AS network conditions are represented by two time series, one is the sum of $d(\Delta)$ over time and the other the sum of r_i over time. In the case of forwarding anomalies, r_i values are negative if a hop from the AS is devalued and positive otherwise. Consequently, if traffic usually goes through a router i but is suddenly rerouted to router j , and both i and j are assigned to the same AS, then the negative r_i and positive r_j values cancel out, thus the anomaly is mitigated at the AS level.

6.2 Event detection

Finding major network disruptions in an AS is done by identifying peaks in either of the two time series described above. We implement a simple outlier detection mechanism to identify these peaks.

Let $X = \{x_t | t \in \mathbb{N}\}$ be a time series representing delay changes or forwarding anomalies for a certain AS and $mag(X)$ be the magnitude of the AS network alteration defined as:

$$mag(X) = \frac{X - \text{median}(X)}{1.4826 \text{MAD}(X)} \quad (11)$$

where median and MAD are the one-week sliding median and median absolute deviation which are usual operators for outlier detection [44]. In the following sections we report maximum magnitude scores for a few ASs and investigate corresponding network disruptions.

7. RESULTS

Using traceroutes from RIPE Atlas (Section 2), we monitored delays for 262k IPv4 links (42k IPv6 links). On average links are observed by 147 IPv4 probes (133 IPv6 probes) and 33% of the links were reported at least once to have an abnormal delay change.

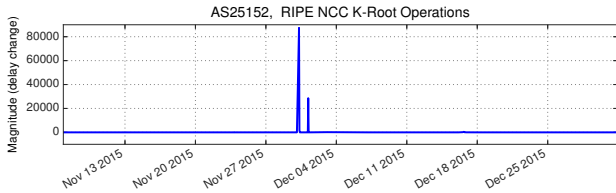


Figure 5: Delay change magnitude for AS25152 reveals the two DDoS against the K-root server.

We also computed packet forwarding models for 170k IPv4 router IPs (87k IPv6 routers). These are the number of router IP addresses found in traceroutes; we are not doing IP aliasing [21]. On average forwarding models contain four different next hops over the eight months of data.

To validate that the error added by return paths (e.g. ϵ_{PBC} in Equation 3) is mitigated even with a small number of probes, we make the following hypothesis. Links where the error is not mitigated are reported more frequently as their differential RTTs account also for links on the return path. However, we found a weak positive correlation (0.24) between the average number of reported alarms and the number of probes monitoring a link. Meaning that links observed by a small number of probes are slightly less reported than those observed by a large number of probes. Furthermore, in accordance with the central limit theorem, we observe a narrower confidence interval for links visited by numerous probes; hence a better differential RTT estimation and the ability to detect smaller delay changes.

We now investigate three case studies showing the relevance of the proposed methods to detect and locate network disruptions of different types.

7.1 DDoS attack on DNS root servers

Our first case-study shows the impact of a large distributed denial-of-service attack (DDoS) attack on network infrastructure. The simplest form of DDoS attacks consists of sending a huge number of requests to a targeted service, overwhelming the service and leaving little or no resources for legitimate use. The extremely large amount of traffic generated by this type of attack is not only detrimental to the victim but also routers in its proximity.

We investigate network disruptions caused by two DDoS attacks against DNS root servers. These attacks have been briefly documented by root server operators [34, 43]. The first attack was on November 30th from 06:50 to 09:30 UTC, the second on December 1st from 05:10 until 06:10 UTC. As the source IP addresses for both attacks were spoofed, it is unclear from reports [43] where the traffic originated.

Thanks to the K-root operators, we were able to care-

fully validate our results for the attack toward the K name server and the corresponding AS (AS25152).

7.1.1 Event detection

Monitoring the delay change magnitude for AS25152 clearly shows the two attacks against the K-root infrastructure (Figure 5). The two peaks on November 30th and December 1st highlight important disruptions of an unprecedented level. The first peak spans from 07:00 to 09:00 UTC and the second one from 05:00 to 06:00 UTC, which correspond to the intervals reported by many server operators.

The highest magnitude forwarding anomaly for AS25152 is recorded on November 30th at 08:00 and is negative ($mag(X) = -6.8$), meaning that packets usually going to this AS have been dropped during the attacks. For these events, the impact on packet forwarding is several orders of magnitude lower than the impact on delay change. These observations match the server operators’ reports and emphasize the help of anycast in mitigating such attacks.

7.1.2 In-depth analysis: K-root

A key advantage of our proposed method is to report delay changes per link, allowing us to precisely locate the effects of the two attacks in the network. Reported delay changes contain one IP address for each end of the link. Delay changes detected on the last hop to the K-root server are identified by the server IP address (193.0.14.129) and the router in front of it. Since K-root is anycast, the actual location of the reported server instance is revealed by locating the adjacent router. For example, Figure 6a depicts the differential RTT for an IP pair composed of the K-root IP address and a router located in Kansas City; hence this link represents the last hop to the K-root instance in Kansas City.

During the two attacks we saw alarms from 23 unique IP pairs containing the K-root server address. Different instances were impacted differently by the attacks. First, we found instances affected by both attacks, for example the one in Kansas City (Figure 6a) is reported during the entire period of time documented by server operators. Second, we also observed instances impacted by only one attack, see Figure 6c. The most reported instance during that period is the one deployed in St. Petersburg (Figure 6d). For this instance abnormal delays are observed for 14 consecutive hours. A possible explanation for this is that hosts topologically close to this instance caused anomalous network conditions for a longer period of time than other reported DDoS intervals. Finally, thanks to anycast, for some instances we did not record anomalous network conditions. Figure 6b illustrates the differential RTT for an instance in Poland that exhibits very stable delays. The corresponding normal reference is exceptionally narrow and

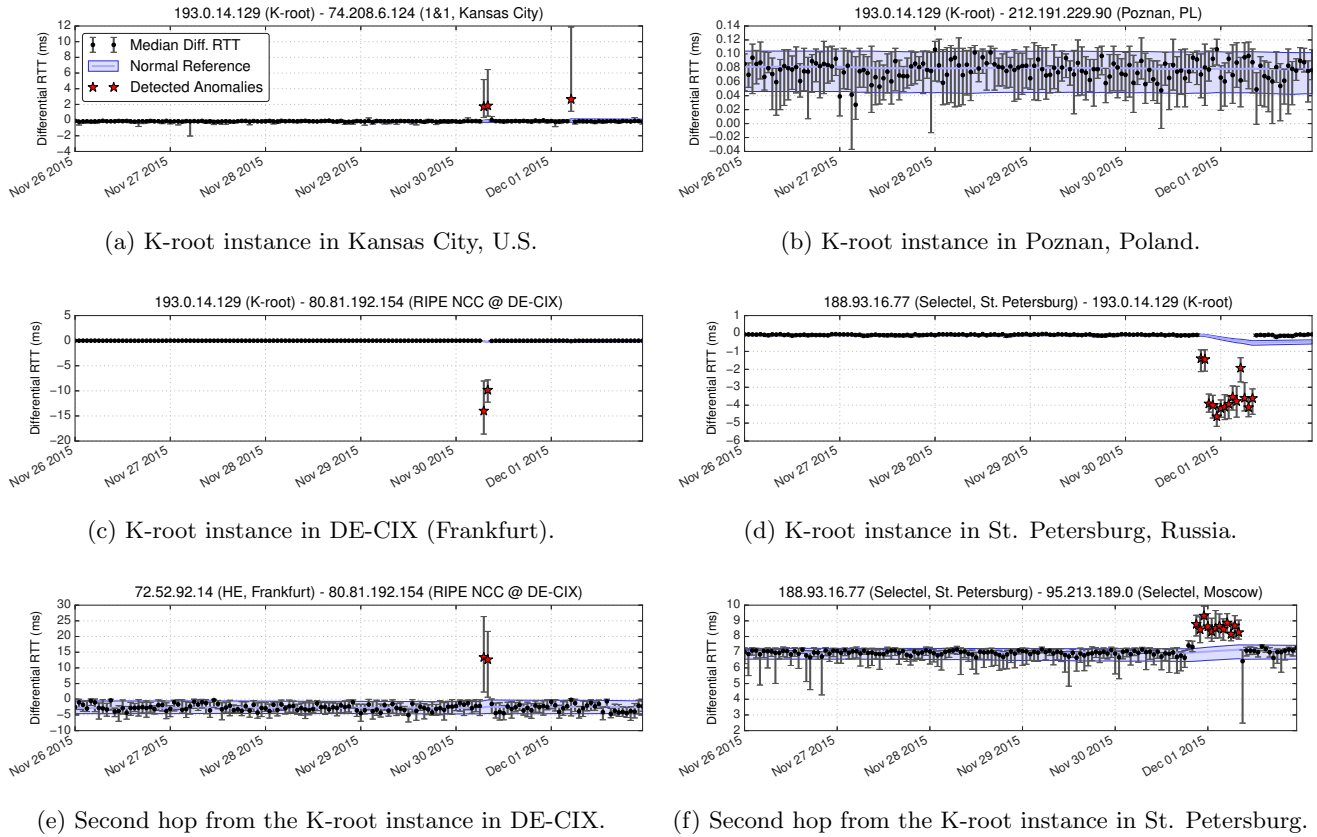


Figure 6: Examples of delay change alarms reported during the DDoS attacks against DNS root servers. The attacks have differently impacted the connectivity of K-root server instances.

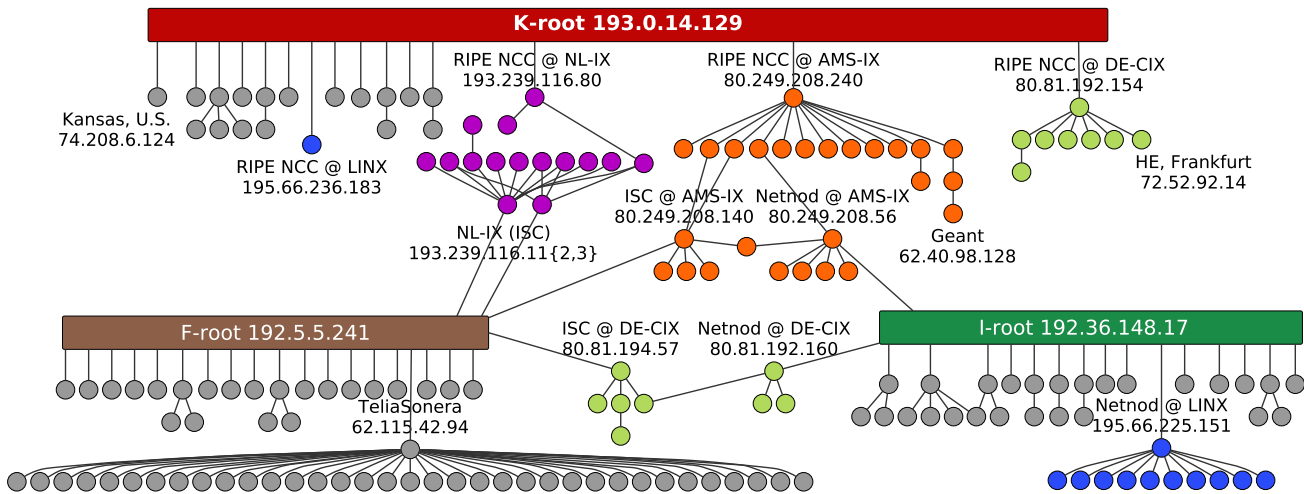


Figure 7: Alarms reported on November 30th at 08:00 UTC and related to the K-root server. Each node represent an IPv4 address, edges stand for reported alarms. Rectangular nodes represent anycast addresses, hence distributed infrastructure. Circular node colors represent IP addresses related to certain IXPs.

constant even during the attacks.

Not only are the last hops to K-root instances detected by our method; we also observe other links with important delay changes. Figure 6e depicts a link in the Deutscher Commercial Internet Exchange (DE-CIX) which is upstream of the K-root instance in Frankfurt (Figure 6c). This link between Hurricane-Electric (AS6939) and the K-root AS exhibits a 15ms delay change (difference between the median differential RTT and the reference median) during the first attack. The upstream link of the instance in St.Petersburg (Figure 6f) is also significantly altered during the attack and is consistent with the peculiar changes observed for this instance (Figure 6d). In certain cases, we observed effects of the attack even further upstream. For example, we observe 7.5ms delay change on a link in the Geant network three hops away from the K-root server (see *Geant 62.40.98.128* in Figure 7).

To assess the extent of the attacks on the network, we create a graph, where nodes are IP addresses and links are alarms generated from differential RTTs between these IP addresses. Starting from the K-root server, we note alarms with common IP addresses and obtain a connected component of all alarms connected to the K-root server. Figure 7 depicts the connected component involving K-root for delay changes detected on November 30th at 08:00 UTC. An anycast address is illustrated by a large rectangular node, because it represents several physical systems. Figure 7 does not show the physical topology of the network but a logical IP view of reported alarms. Each edge to an anycast address usually represents a different instance of a root server. There are rare cases where two edges may represent the same instance, for example, the K-root instance available at AMS-IX and NL-IX is actually the same physical cluster. Some of the alarms mentioned above and illustrated in Figure 6a, 6c, and 6e are also displayed in Figure 7. The shape of the graph reveals the wide impact of the attack on network infrastructure. It also shows that alarms reported for the K-root servers are adjacent to the ones reported for the F and I-root servers. This is due to the presence of all three servers at the same exchange points; hence some network devices are affected by malicious traffic targeting other root servers. The concentration of root servers is of course delicate in this situation. Nonetheless, the low number of forwarding anomalies indicates that routers at the IXPs could handle the load but at the expense of delay increases.

Additional root servers are represented by different connected components. During the three hours of attack there were 129 alarms involving root servers for IPv4 (49 for IPv6). In agreement with the observations made by servers operators [43], we observed no significant delay change for root servers A, D, G, L, and M.

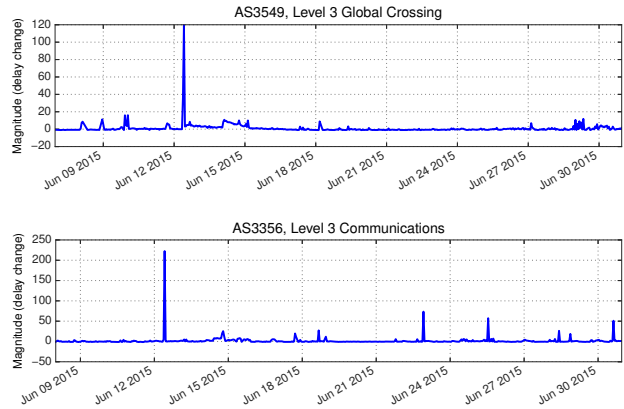


Figure 8: Delay change magnitude for all monitored IP addresses in two Level(3) ASs.

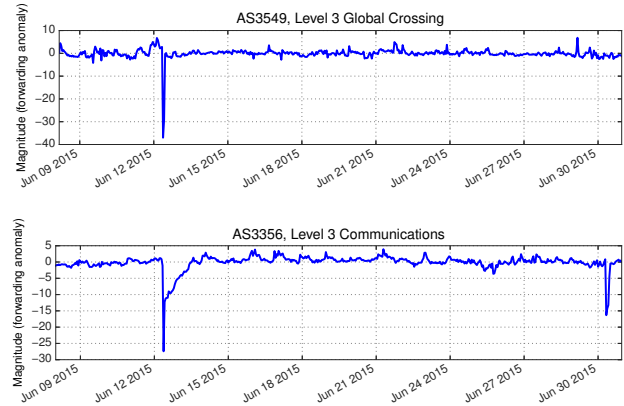
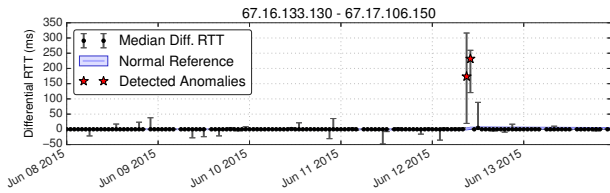


Figure 9: Forwarding anomaly magnitude for all monitored IP addresses in two Level(3) ASs.

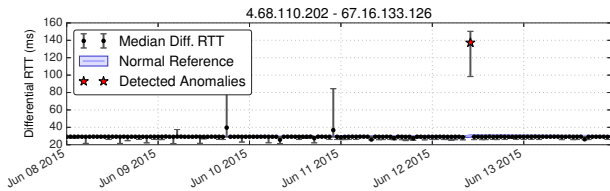
7.2 Telekom Malaysia BGP route leak

The above example of the K-root servers illustrates the benefits of our delay change detection method to detect anomalies near a small AS at the edge. In this section we investigate network disruptions for a tier 1 ISP showing that the methods also enable us to monitor large ASs containing numerous links. This case study also exposes a different type of network disruption; here the detected anomalies are caused by abnormal traffic rerouting.

On June 12th 2015, 08:43 UTC, Telekom Malaysia (AS4788) unintentionally sent BGP announcements for numerous IP prefixes to its provider Level(3) Global Crossing (AS3549) which accepted them. The resulting traffic attraction to Telekom Malaysia caused latency increases for Internet users all over the globe. The event was acknowledged by Telekom Malaysia [3], and independently reported by BGP monitoring projects [41, 20]. Connectivity issues have been mainly attributed



(a) London-London link: delay change reported on June 12th at 09:00 and 10:00 UTC.



(b) New York-London link: delay change reported at 10:00 UTC. RTT samples for June 12th at 09:00 UTC are missing due to forwarding anomaly (packet loss).

Figure 10: Example of delay change alarms reported during the Telekom Malaysia BGP route leak for two links from Level3 networks.

to congested peering links between Telekom Malaysia and Level(3) Global Crossing. In the remainder of this section we investigate the impact of rerouted traffic on Level(3) Global Crossing (AS3549) and its parent company, Level(3) Communications (AS3356), showing worldwide disruptions.

7.2.1 Network disruptions in Level(3)

Monitoring delay changes and forwarding anomalies for the numerous links that constitute the two Level(3) ASs is made easy with the magnitude metric (Equation 11). Figure 8 and 9 depict the magnitude in terms of, respectively, delay change and forwarding anomaly for the two Level(3) ASs in June 2015. The two positive peaks in Figure 8 and the two negative peaks in Figure 9 are all reported on June 12th from 09:00 to 11:00 UTC, exposing the impact of rerouting on both ASs. The overall delay increased for both ASs, but AS3549 was most affected. The negative forwarding anomaly magnitudes (Figure 9) show that routers from both ASs were disappearing abnormally from the forwarding model obtained by traceroutes. At the same time packet loss increased, implying that numerous routers from both ASs dropped a lot of packets.

7.2.2 In-depth analysis

Reverse DNS lookups of reported IP addresses suggests congestion was seen in numerous cities, including, Amsterdam, Berlin, Dublin, Frankfurt, London, Los Angeles, Miami, New York, Paris, Vienna, and Washington, for both Level(3) ASs. Figure 10 shows the

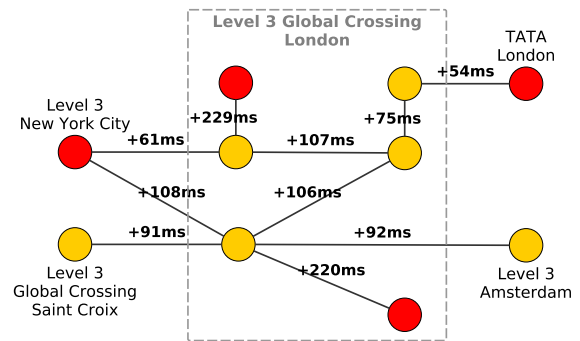


Figure 11: Congestion at Level(3) Global Crossing (AS3549) in London on June 12th 2015. Each node represents an IPv4 address, edges represent delay changes for an IP pair. Red nodes depict IP addresses involved in forwarding anomalies.

differential RTT obtained for two links located in New York and London. Both links exhibit significant delay increases synchronous with the Telekom Malaysia route leak. The London-London link (Figure 10a) is reported from 09:00 to 11:00 UTC, while the New York-London link (Figure 10b) is reported from 10:00 to 11:00 UTC. The IP address identified in New York is found in forwarding anomalies, and is suspected of dropping probing packets from 09:00 to 10:00 UTC; hence preventing the collection of RTT samples for this link. This example illustrates the complementarity of the delay change and forwarding anomaly detection methods.

As in the case of the K-root servers, several adjacent links are reported at the same time. Figure 11 shows related components of alarms reported on June 12th at 10:00 UTC in London. The label on each edge is the absolute difference between the observed median differential RTT and the median of the normal reference. The links in Figure 10a and 10b are marked by delay changes of, respectively, $+229ms$ and $+108ms$. Similar observations are made for the two Level(3) ASs and numerous cities mainly in U.S. and Europe. Consequently, even non-rerouted traffic going through Level(3) at that time could also incur significant latency increase and packet loss.

7.3 Amsterdam Internet Exchange Outage

The first two study cases presented network disruptions with significant delay changes. Here we introduce an example of network disruption but only visible through forwarding anomalies; showing the need for both delay change and forwarding anomaly detection methods. In this example the disruption is caused by a technical fault in an Internet exchange resulting in extensive connectivity issues.

On May 13th 2015 around 10:20 UTC, the Amster-

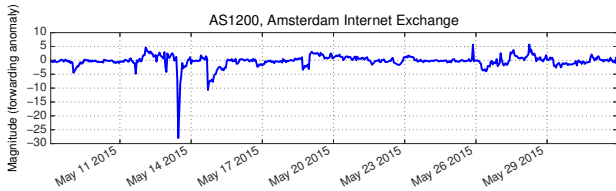


Figure 12: Forwarding anomaly magnitude for the Amsterdam Internet Exchange peering LAN (AS1200).

dam Internet Exchange (AMS-IX) encountered substantial connectivity problems due to a technical issue during maintenance activities. Consequently, several connected networks could not exchange traffic through the AMS-IX platform; hence a number of Internet services were unavailable [2]. AMS-IX reported that the problem was solved at 10:30 UTC; but traffic statistics indicate that the level of transmitted traffic did not return to normal until 12:00 UTC [22, 5].

7.3.1 Event detection

Our delay change method didn’t conclusively detect this outage, due to RTT samples lacking during the outage. This was likely due to traffic being dropped before it crossed the AMS-IX peering fabric. The packet loss rate, however, showed significant disturbances at AMS-IX. These changes were captured by our packet forwarding model as a sudden disappearance of the AMS-IX peering LAN for many neighboring routers. Consequently, forwarding anomalies with negative responsibility scores (Equation 10) were synchronously reported for IP addresses in the AMS-IX peering LAN. Monitoring the magnitude for the corresponding AS (Figure 12) reveals these changes as a significant negative peak on May 13th 11:00 UTC. Further, the coincidental surge of unresponsive hops reported by forwarding anomalies supports the fact that traffic was not rerouted but dropped.

The packet forwarding model allows us to precisely determine peers that could not exchange traffic during the outage. In total 770 IP pairs related to the AMS-IX peering LAN became unresponsive. Therefore, the proposed method to learn packet forwarding patterns and systematically identify unresponsive IP addresses greatly eases the understanding of such an outage.

8. DISCUSSION

The methods proposed in this paper complement the literature by circumventing common problems found in past works. With the help of the packet forwarding model, we take advantage of all collected traceroutes including even those that are incomplete due to packet loss. Also, as we do not rely on any IP or ICMP options,

the number of monitored routers is superior to previous work. In fact, our statistical approach allows us to study any link with routers responding to traceroute and that can be seen by at least three probes hosted in different ASs. Therefore, the number of monitored links mainly depends on the placement of probes and the selected traceroute destinations. In other words, using our techniques the number of monitored links is given by the measurement setup rather than the router’s implementation. In our experiments we could monitor links from 1060 ASs. Stub ASs hosting probes but no traceroute targets were not monitored as they were observed only by probes from the same AS. Increasing the number of traceroute targets could however significantly increase the number of monitored ASs.

The proposed methods, however, suffer from common limitations faced by traceroute data [24, 35, 23]. Traceroute visibility is limited to the IP space, hence, changes at lower layers that are not visible at the IP layer can be misinterpreted. For example, the RIPE Atlas data reports MPLS information if routers support RFC4950. But for routers that are not supported, the reconfiguration of an MPLS tunnel has long term impact on the delay of a link. In our experiments, we found that this case is characterized by links being reported for an extended period of time until the normal reference is adjusted to the new delay.

The RTT values reported by traceroute include both network delays and routers’ slow path delay [23]. Therefore, the delay changes found using traceroute data are not to be taken as the actual delay increase experienced by Internet users. Nonetheless, delay changes are representative of the router load.

9. CONCLUSIONS

In this paper we investigated the challenges to monitoring network conditions from traceroute results. We then tackled these challenges with a statistical approach that took advantage of large-scale traceroute measurements to accurately pinpoint delay changes and packet loss. Our experiments with the RIPE Atlas platform validate our methods and emphasize the benefits of this approach to characterize topological impacts.

We make our tools and results publicly available¹ in order to share our findings and contribute to a better understanding of Internet reliability.

10. REFERENCES

- [1] RIPE NCC, Atlas. <https://atlas.ripe.net>.
- [2] Follow-up on previous incident at AMS-IX platform. <https://ams-ix.net/newsitems/195>, May 2015.
- [3] Telekom Malaysia: Internet services disruption. <https://www.tm.com.my/OnlineHelp/>

¹ <http://romain.ijlab.net/iwr/reports/>

- [Announcement/Pages/internet-services-disruption-12-June-2015.aspx](#), June 2015.
- [4] E. Aben. Hurricane Sandy as seen by RIPE Atlas. *NANOG 57*, February 2013.
- [5] E. Aben. Does the internet route around damage? a case study using RIPE Atlas. <https://labs.ripe.net/Members/emileaben/does-the-internet-route-around-damage>, November 2015.
- [6] J. Aikat, J. Kaur, F. D. Smith, and K. Jeffay. Variability in TCP round-trip times. In *Proceedings of IMC'03*, pages 279–284. ACM, 2003.
- [7] K. G. Anagnostakis, M. Greenwald, and R. S. Ryger. cing: Measuring network-internal delays using only existing infrastructure. In *INFOCOM 2003*, volume 3, pages 2112–2121. IEEE, 2003.
- [8] B. Augustin, X. Cuvellier, B. Orgogozo, F. Viger, T. Friedman, M. Latapy, C. Magnien, and R. Teixeira. Avoiding traceroute anomalies with Paris traceroute. In *IMC*, pages 153–158. ACM, 2006.
- [9] R. Banerjee, A. Razaghpanah, L. Chiang, A. Mishra, V. Sekar, Y. Choi, and P. Gill. Internet outages, the eyewitness accounts: Analysis of the outages mailing list. In *Passive and Active Measurement*, pages 206–219. Springer, 2015.
- [10] B. Chandrasekaran, G. Smaragdakis, A. Berger, M. Luckie, and K.-C. Ng. A server-to-server view of the internet. In *CoNEXT*. ACM, 2015.
- [11] W. de Donato, P. Marchetta, and A. Pescapé. A hands-on look at active probing using the IP prespecified timestamp option. In *Passive and Active Measurement*, pages 189–199. Springer, 2012.
- [12] W. de Vries, J. J. Santanna, A. Sperotto, and A. Pras. How asymmetric is the internet? a study to support the use of traceroute. In *Intelligent mechanisms for network configuration and security*, volume 9122 of *LNCS*, pages 113–125. Springer, June 2015.
- [13] L. Deng and A. Kuzmanovic. Monitoring persistently congested internet links. In *Network Protocols, 2008. ICNP 2008. IEEE International Conference on*, pages 167–176. IEEE, 2008.
- [14] S. Floyd and V. Jacobson. Random early detection gateways for congestion avoidance. *Networking, IEEE/ACM Transactions on*, 1(4):397–413, 1993.
- [15] R. Fontugne, J. Mazel, and K. Fukuda. An empirical mixture model for large-scale RTT measurements. In *INFOCOM'15*, pages 2470–2478. IEEE, 2015.
- [16] J. D. Gibbons and S. Chakraborti. Nonparametric statistical inference. 2011.
- [17] Y. Gu, L. Breslau, N. Duffield, and S. Sen. On passive one-way loss measurements using sampled flow statistics. In *INFOCOM 2009, IEEE*, pages 2946–2950. IEEE, 2009.
- [18] E. Katz-Bassett, J. P. John, A. Krishnamurthy, D. Wetherall, T. Anderson, and Y. Chawathe. Towards IP geolocation using delay and topology measurements. In *Proceedings of IMC'06*, pages 71–84. ACM, 2006.
- [19] E. Katz-Bassett, H. V. Madhyastha, V. K. Adhikari, C. Scott, J. Sherry, P. Van Wesep, T. E. Anderson, and A. Krishnamurthy. Reverse traceroute. In *NSDI*, volume 10, pages 219–234, 2010.
- [20] N. Kephart. Route leak causes global outage in level 3 network. <https://blog.thousandeyes.com/route-leak-causes-global-outage-level-3-network/>, June 2015.
- [21] K. Keys, Y. Hyun, M. Luckie, and K. Claffy. Internet-scale ipv4 alias resolution with midar. *IEEE/ACM Transactions on Networking (TON)*, 21(2):383–399, 2013.
- [22] R. Kisteleki. The AMS-IX outage as seen with RIPE Atlas. <https://labs.ripe.net/Members/kistel/the-ams-ix-outage-as-seen-with-ripe-atlas>, May 2015.
- [23] M. Luckie, A. Dhamdhare, D. Clark, B. Huffaker, and k. claffy. Challenges in inferring internet interdomain congestion. In *IMC*, pages 15–22. ACM, 2014.
- [24] M. Luckie, Y. Hyun, and B. Huffaker. Traceroute probe method and forward IP path inference. In *IMC*, pages 311–324. ACM, 2008.
- [25] R. Mahajan, N. Spring, D. Wetherall, and T. Anderson. User-level Internet path diagnosis. *SOSP'03*, 37(5):106–119, 2003.
- [26] V. Manojlovic. Using RIPE Atlas and RIPEstat to detect network outage events. *SANOG 27*, January 2016.
- [27] P. Marchetta, A. Botta, E. Katz-Bassett, and A. Pescapé. Dissecting round trip time on the slow path with a single packet. In *PAM*, pages 88–97. Springer, 2014.
- [28] A. Markopoulou, F. Tobagi, and M. Karam. Loss and delay measurements of internet backbones. *Computer Communications*, 29(10):1590–1604, 2006.
- [29] R. G. Newcombe. Two-sided confidence intervals for the single proportion: comparison of seven methods. *Statistics in medicine*, 17(8):857–872, 1998.
- [30] P. Owen, A. Schulman, and N. Spring. Timeouts:

- Beware surprisingly high delay. In *IMC*, pages 303–316. ACM, 2015.
- [31] C. Pelsser, L. Cittadini, S. Vissicchio, and R. Bush. From Paris to Tokyo: on the suitability of ping to measure latency. In *Proceedings of IMC'13*, pages 427–432. ACM, 2013.
- [32] L. Quan, J. Heidemann, and Y. Pradkin. Trinocular: Understanding Internet reliability through adaptive probing. In *Proceedings of the ACM SIGCOMM Conference*, pages 255–266, Hong Kong, China, August 2013. ACM.
- [33] L. Rizo-Dominguez, D. Munoz-Rodriguez, C. Vargas-Rosales, D. Torres-Roman, and J. Ramirez-Pacheco. RTT prediction in heavy tailed networks. *IEEE Communications Letters*, 18(4):700–703, April 2014.
- [34] Root Server Operators. Events of 2015-11-30. <http://www.root-servers.org/news/events-of-20151130.txt>, December 2015.
- [35] M. Roughan, W. Willinger, O. Maennel, D. Perouli, and R. Bush. 10 lessons from 10 years of measuring and modeling the internet’s autonomous systems. *Selected Areas in Communications, IEEE Journal on*, 29(9):1810–1821, 2011.
- [36] N. Schenker and J. F. Gentleman. On judging the significance of differences by examining the overlap between confidence intervals. *The American Statistician*, 55(3):182–186, 2001.
- [37] Y. Schwartz, Y. Shavitt, and U. Weinsberg. On the diversity, stability and symmetry of end-to-end Internet routes. In *INFOCOM IEEE Conference on Computer Communications Workshops, 2010*, pages 1–6. IEEE, 2010.
- [38] A. Singla, B. Chandrasekaran, P. Godfrey, and B. Maggs. The internet at the speed of light. In *Proceedings of the 13th ACM Workshop on Hot Topics in Networks*, page 1. ACM, 2014.
- [39] J. Sommers, P. Barford, N. Duffield, and A. Ron. Improving accuracy in end-to-end packet loss measurement. *ACM SIGCOMM Computer Communication Review*, 35(4):157–168, 2005.
- [40] R. Teixeira, K. Marzullo, S. Savage, and G. M. Voelker. In search of path diversity in ISP networks. In *Proceedings of the 3rd ACM SIGCOMM conference on Internet measurement*, pages 313–318. ACM, 2003.
- [41] A. Toonk. Massive route leak causes internet slowdown. <http://www.bgpmon.net/massive-route-leak-cause-internet-slowdown/>, June 2015.
- [42] F. Wang, Z. M. Mao, J. Wang, L. Gao, and R. Bush. A measurement study on the impact of routing events on end-to-end internet path performance. *ACM SIGCOMM Computer Communication Review*, 36(4):375–386, 2006.
- [43] M. Weinberg and D. Wessels. Review and analysis of attack traffic against A-root and J-root on November 30 and December 1, 2015. *OARC 24*, April 2016.
- [44] R. R. Wilcox. *Fundamentals of Modern Statistical Methods: Substantially Improving Power and Accuracy*. Springer Science & Business Media, 2010.
- [45] E. B. Wilson. Probable inference, the law of succession, and statistical inference. *Journal of the American Statistical Association*, 22(158):209–212, 1927.
- [46] B. Zhang, T. Ng, A. Nandi, R. H. Riedi, P. Druschel, and G. Wang. Measurement-based analysis, modeling, and synthesis of the Internet delay space. *IEEE/ACM Transactions on Networking*, 18(1):229–242, Feb 2010.
- [47] M. Zhang, C. Zhang, V. S. Pai, L. L. Peterson, and R. Y. Wang. Planetseer: Internet path failure monitoring and characterization in wide-area services. In *OSDI*, volume 4, pages 12–12, 2004.
- [48] H. Zheng, E. K. Lua, M. Pias, and T. G. Griffin. Internet routing policies and round-trip-times. In *Passive and Active Network Measurement*, pages 236–250. Springer, 2005.